Neutron isotopic density differences deduced from 0.8 GeV polarized proton elastic scattering

L. Ray
Theoretical Division, University of California, Los Alamos Scientific Laboratory, Los Alamos, New Mexico 87545
(Received 15 January 1979)

The microscopic spin-independent proton-nucleus optical potential defined by Kerman, McManus, and Thaler is used to analyze recent 0.8 GeV polarized proton elastic scattering data from ^{40,48}Ca, ^{58,64}Ni, ^{116,124}Sn, and ^{208}Pb. Second-order effects due to target nucleon correlations are included in both the central and spin-orbit parts of the proton-nucleus optical potential. Electromagnetic corrections to the proton density which arise from the electric and magnetic form factors of the neutron, and from the magnetic form factor of the proton, are also calculated. A discussion is presented regarding uncertainties in the nucleon-nucleon amplitudes used in construction of the potential, and also discrete ambiguities which arise from fitting the limited set of nucleon-nucleon data available near 1 GeV are examined. Approximately model-independent forms are assumed for the target neutron density distributions, thereby allowing the statistical and model-dependence errors to be estimated. Neutron density and rms radii are deduced and compared to Hartree-Fock predictions, with good agreement found for most of the seven nuclei studied. Because of the uncertainty in the proton-nucleon amplitudes, neutron density and radius differences are considered more reliable than individual absolute values. Owing to the inclusion of certain second-order terms discussed here, an accurate determination of these differences is obtained.

[NUCLEAR REACTIONS proton-nucleus scattering, $E_p = 0.8$ GeV; targets ^{40,48}Ca, ^{58,64}Ni, ^{116,124}Sn, and ^{208}Pb; Kerman, McManus and Thaler optical potential; target nucleon correlations; electromagnetic corrections; deduced neutron density distributions and radii.]

I. INTRODUCTION

In recent months a considerable amount of high quality, polarized proton scattering data at 0.8 GeV[1-4] has become available to theorists interested in examining nuclear matter density distributions,[2-7] correlation effects,[7-12] and the spin-dependence of both the proton-nucleus and the proton-nucleon scattering amplitudes.[2,6] The principal improvement of this new data, obtained with the high resolution spectrometer (HRS) at the Clinton P. Anderson Meson Physics Facility (LAMPF), in comparison to the earlier 1.0 GeV proton scattering data obtained at Saclay[13-15] and Gatchina,[16] is its high statistical quality,[1] its extension to high momentum transfer,[1,3] the excellent angular resolution and absolute angle determination,[1,2,6] and the inclusion of elastic analyzing power data.[1-4] The good statistical quality and high momentum transfer of these data provide greater sensitivity to the shape of the nuclear density, particularly in the surface region.[5,6] The great accuracy with which the absolute scattering angle has been determined for the 0.8 GeV data ($\cong \pm 0.03°$)[1] is vital for studies of neutron matter sizes since such an error contributes significantly to the radius uncertainty (i.e., $\cong \pm 0.08$ fm/0.1° of absolute angle uncertainty).[6] Simultaneous analysis of cross section and analyzing power data allows the determination of effective proton-nucleon spin-orbit amplitudes[2,6] and thereby eliminates a moderate source of uncertainty in the deduced neutron radii (i.e., $\cong \pm 0.03$ fm).[5]

Initially these data were analyzed with the optical potential formalism of Kerman, McManus, and Thaler (KMT)[17] and Feshbach and his collaborators[18,19] using a first order, $t(q^2)\tilde{\rho}(q^2)$-type optical potential. In other words, corrections due to target nucleon correlations,[7-12] nuclear center-of-mass to proton-nucleus c.m. transformations[11] and electromagnetic corrections to the proton matter density[20] were neglected. With the appearance of excellent data, such as that obtained at LAMPF, more careful calculations are called for.

Presented in this work are the results of a microscopic optical potential analysis in which target nucleon correlations[7-12] and center-of-mass transformations[11] are included to second order in the nuclear density and in which the leading corrections to the point-proton density due to the neutron's electric and magnetic form factors and the proton's magnetic moment are included.[20] In addition, approximately model-independent forms[6] for the neutron matter densities, $\rho_n(r)$, are used, thereby allowing the uncertainties in $\rho_n(r)$ due to statistical error and model dependence[21,22] to be estimated. Various experimental and systematic errors which deter the accurate determination of neutron matter radii are also considered in estimating the total uncertainty in $\rho_n(r)$.

Before completely reliable determinations of neutron densities with hadronic probes can be

achieved, the scattering theory used must be thoroughly tested. Exhaustive tests of the accuracy of the KMT optical potential approach, or of the multiple scattering diffraction theory of Glauber[23] in determining neutron matter radii or shapes is lacking. The most severe obstruction to such tests is the fact that the fundamental two-nucleon amplitudes needed as input in either calculation are not well known at these energies.[24-37] The uncertainty of the two-nucleon amplitudes is not simply a matter of model dependence or the variation allowed in fitting the forward angle $p+p$ or $p+n$ data.[6] The effect that these errors have on the deduced neutron radius have been estimated[5,6] and are quite small ($\cong \pm 0.03$ fm). The more serious problem involves arbitrary assumptions (due to the lack of N-N data) about double-spin-flip amplitudes and the occurrence of discrete ambiguities in fitting the N-N cross section and polarization data available at ~1 GeV. These difficulties, which will be discussed in detail in the next section, have motivated the present study, which concentrates primarily on obtaining accurate *relative differences* between the neutron radii and distributions of nuclei in several isotopic sequences. The specific cases considered are ^{40,48}Ca, ^{58,64}Ni, and ^{116,124}Sn, all obtained at LAMPF[2-4] using the 0.8 GeV, polarized proton beam. To span the mass range of data obtained at LAMPF, the results for ^{208}Pb will also be included.[1]

In Sec. II a brief outline of the KMT optical potential formalism is given, the assumptions made in obtaining the two-nucleon scattering amplitudes are explained, and the several corrections required to determine the point proton density accurately from empirical charge densities are discussed. Also the approximations made in estimating the correlation corrections and the approximately model-independent neutron densities used are given in Sec. II. In Sec. III the numerical results of this analysis are presented. Deduced values for the neutron-proton rms radius difference, isotopic neutron radii differences, and the associated errors, are given and compared to Hartree-Fock predictions.[38] The neutron density distributions, $\rho_n(r)$, and the relative differences between isotopes, $\Delta\rho_n(r)$, along with the estimated uncertainties, are displayed in this section together with Hartree-Fock predictions.[38] A summary and some conclusions will finally be given in Sec. IV.

II. GENERAL DETAILS OF THE KMT OPTICAL POTENTIAL ANALYSIS

In the optical potential approach of Kerman, McManus, and Thaler[17] the full nucleon-nucleus t matrix is expressed in terms of the fundamental two-nucleon scattering amplitudes in an iterative series. This is obtained by manipulating the Lippmann-Schwinger operator equation for this t matrix into a form from which the proton-nucleus optical potential can be identified. This optical potential has been expressed most lucidly by Feshbach, *et al.*[18] as a "multiple excitation" series which involves all orders of nuclear and nucleon intermediate excitations and is given by

$$U^{\rm opt} = U_{00} + \sum_{\alpha \neq 0}^{\infty} U_{0\alpha} \frac{1}{E^{(+)} - \epsilon_\alpha - K - U_{\alpha\alpha} + i\delta} U_{\alpha 0} + \cdots , \tag{1}$$

where $E^{(+)}$ and ϵ_α are the projectile and intermediate nuclear energies, respectively, as explained in Ref. 18 and where

$$U_{\alpha\beta} = (A-1)\langle \phi_\alpha | \tau | \phi_\beta \rangle . \tag{2}$$

In Eq. (2), $|\phi_\alpha\rangle$ is the wave function of the excited nuclear level α, and τ is given by

$$\tau = v + v \frac{\mathcal{A}}{E^{(+)} - K - H_N + i\delta} \tau . \tag{3}$$

In this last equation, v is the two-nucleon interaction and τ represents the two-nucleon t matrix evaluated in the target nucleus of A nucleons whose full Hamiltonian is given by H_N. The antisymmetrization projection operator, $\mathcal{A}$, allows only physical states of the nucleus as intermediate states.

If it is assumed that the two-nucleon amplitude depends only weakly on the momentum of the target nucleon then Eq. (2) can be simplified to obtain[18]

$$\tilde{U}_{\alpha\beta}(q^2) \cong (A-1)\tau(q^2) F_{\alpha\beta}(q^2) , \tag{4}$$

where q is the momentum transfer. Such a factorization is valid provided the N-N amplitudes do not vary too rapidly over an energy range of about ~100 MeV around the incident beam energy. This condition is reasonably well satisfied by the N-N amplitudes at energies near ~1 GeV, and hence should be valid in this energy regime, as is discussed more fully by Chaumeaux *et al.*[11] In Eq. (4) the form factor $F_{00}(q^2)$, would, for example, be the momentum-transfer-space representation of the nuclear ground state density. If one replaces $\tau(q^2)$ with the free nucleon-nucleon amplitude $t(q^2)$[24] and includes the leading (τ-t) correction in the second term of Eq. (1) then as derived by Feshbach *et al.*,[18] the nucleon-nucleus optical potential can be expressed to second order as

$$U^{\rm opt} \cong (A-1)\left\langle \frac{1}{A}\sum_i t_i \right\rangle_{00} + (A-1)^2 \left[\frac{1}{A(A-1)} \sum_{i\neq j} \left\langle t_i \frac{1}{\bar{\alpha}} t_j \right\rangle_{00} - \left\langle \frac{1}{A}\sum_i t_i \right\rangle_{00} \frac{1}{\bar{\alpha}} \left\langle \frac{1}{A}\sum_j t_j \right\rangle_{00} \right], \quad (5)$$

where $\bar{\alpha} = \langle \beta | E^{(+)} - K - H_N - (A-1)\tau | \beta \rangle$ is assumed to be independent of the intermediate nuclear state $|\beta\rangle$ and the usual closure approximation has been made.[17,18] The notation $\langle\ \rangle_{00}$ means $\langle \phi_0 |\ |\phi_0\rangle, |\phi_0\rangle$ being the nuclear ground-state wave function. The second term in this equation is proportional to the two-body correlation function.[7-12]

From this last equation it is seen that the ingredients in these calculations are: (1) the free two-nucleon scattering amplitudes, (2) the ground-state proton and neutron one-body densities, and (3) the two-body correlation functions. When one has thus obtained $U^{\rm opt}$, it is inserted into a Schrödinger equation which includes relativistic kinematics as in Ref. 39. The final differential cross section is then obtained from $|T|^2$, where $T = AT'/(A-1)$ and T' is the on-shell, proton-nucleus t matrix obtained from the solution of the Schrödinger equation.

In the remainder of this section the assumptions made in determining the two-nucleon amplitudes, the details of extracting the point proton density from the nuclear charge distribution, the approximations used to estimate the second order terms, and a summary of the approximately model-independent method for evaluating the one-body neutron densities will be given.

A. The two-nucleon input

A general form for the two-nucleon scattering amplitudes consistent with space reflection, rotation, and time-reversal invariances is[24]

$$t_{pj}(q^2) = t^0_{pj}(q^2) + i t^s_{pj}(q^2)(\vec{\sigma}_p + \vec{\sigma}_j)\cdot\hat{n} + m(q^2)(\vec{\sigma}_p\cdot\hat{n})(\vec{\sigma}_j\cdot\hat{n}) + g(q^2)[(\vec{\sigma}_p\cdot\hat{P})(\vec{\sigma}_j\cdot\hat{P}) + (\vec{\sigma}_p\cdot\hat{K})(\vec{\sigma}_j\cdot\hat{K})] + h(q^2)[(\vec{\sigma}_p\cdot\hat{P})(\vec{\sigma}_j\cdot\hat{P}) - (\vec{\sigma}_p\cdot\hat{K})(\vec{\sigma}_j\cdot\hat{K})], \quad (6)$$

where $\hat{n} = (\vec{k}_i \times \vec{k}_f)/|\vec{k}_i \times \vec{k}_f|$, $\hat{P} = (\vec{k}_i + \vec{k}_f)/|\vec{k}_i + \vec{k}_f|$, $\hat{K} = (\vec{k}_f - \vec{k}_i)/|\vec{k}_f - \vec{k}_i|$, and p refers to the incident proton, while $j = p$ or n denotes the target nucleon.

In general these five complex quantities must be known over the same momentum transfer range covered by the proton-nucleus data. For scattering from spin 0 nuclei, only the t^0_{pj} and t^s_{pj} amplitudes enter in the first-order calculation.[40] However, these two amplitudes cannot be determined independently from the other three amplitudes by any simple subset of nucleon-nucleon experiments. All five amplitudes have to be determined in order to obtain any particular one uniquely. To do this requires nine experiments for both the $p+p$ and $p+n$ systems[41] and such experimental information is not available at energies near 1 GeV.[25,26] Therefore, one must make a number of simplifying assumptions and analyze the data that do exist, namely elastic cross section and polarization data.[25-31]

Chaumeaux, Layly, and Schaeffer[11] argue that the "double-spin-flip" amplitudes m, g, and h in Eq. (6) should be negligible compared to $t^0_{pj}(q^2)$ and that $t^s_{pj}(q^2)$ is primarily determined by the N-N polarization data. Neglecting these double-spin-flip amplitudes may or may not be a good approximation, at least for the $p+p$ system, in light of the recent polarized total cross section differences measured at Argonne.[42,43] However, until the two-nucleon amplitudes are fully known one is forced to work only with the first two terms in Eq. (6).

The forms customarily assumed for these amplitudes at energies near 1 GeV are[1-6]

$$t^0_{pj}(q^2) = (ik_0\sigma^T_{pj}/4\pi)(1 - i\alpha_{pj})\exp(-B_{pj}q^2),$$
$$t^s_{pj}(q^2) = (ik_0\theta_{pj}/4\pi)(1 - i\alpha_{spj})(q^2/4M^2)^{1/2} \times \exp(-B_{spj}q^2), \quad (7)$$

where k_0 is the nucleon momentum in the two nucleon center-of-momentum system, σ^T_{pj} is the spin averaged total cross section, and M is the nucleon mass. Various calculations have been made in which B_{pj} is taken to be complex,[11,44] but such generalizations have negligible effect on the resulting proton-nucleus differential cross sections. Also phase shift analysis results for $t^0_{pj}(q^2)$ have been used[45] in proton-nucleus calculations and again insignificant changes are noted.

In Eq. (7) there are a total of 12 parameters to be determined for 800 MeV proton scattering Total cross section measurements[25,26,32] provide $\sigma^T_{pp} = 4.73 \pm 0.05$ fm^2 and $\sigma^T_{pn} = 3.79 \pm 0.022$ fm^2, while very forward angle $p+p$ measurements in the Coulomb-nuclear interference region yield $\alpha_{pp} = 0.06 \pm 0.08$.[33,34] Dispersion theory estimates

give $\alpha_{pn}=-0.3\pm0.15$ at 0.8 GeV.[35-37] Since the value of α_{pj} affects only the peak-to-valley ratio of the diffractive angular distribution and not the angular position of the maxima or minima, its effect on the deduced neutron density is minute.[6] Therefore, the value of α_{pn} has been varied within the above range to obtain the optimal result for the dozen target nuclei studied at 0.8 GeV.[1-5] These range in mass from $A=12$ to $A=208$ with the resultant value for α_{pn} being -0.2. Thus very forward angle measurements and the peak-to-valley ratios in the proton-nucleus angular distribution enable two of the six parameters in Eq. (7) to be fixed for both the p-p and p-n amplitudes.

The four remaining parameters in Eq. (7) must be determined by fitting the available N-N elastic cross section and polarization data. Keeping only the first two terms in Eq. (6) and using the forms in Eq. (7) the two-nucleon elastic cross section and polarization are[24]

$$\frac{d\sigma}{d\Omega}=(\sigma_{pj}^{T}k_0/4\pi)^2(1+\alpha_{pj}^{\,2})\exp(-2B_{pj}q^2)+2(\theta_{pj}k_0/4\pi)^2(1+\alpha_{spj}^{\,2})(q^2/4M^2)\times\exp(-2B_{spj}q^2) \quad (8)$$

and

$$P(d\sigma/d\Omega)=\sigma_{pj}^{T}(k_0/4\pi)^2[\theta_{pj}(\alpha_{spj}-\alpha_{pj})]\times(\hbar cq/Mc^2)\exp[-(B_{spj}+B_{pj})q^2]. \quad (9)$$

The quantity $P(d\sigma/d\Omega)/q$ when computed for the $p+p$ data at 800 MeV[27,28] and for the $p+n$ data at

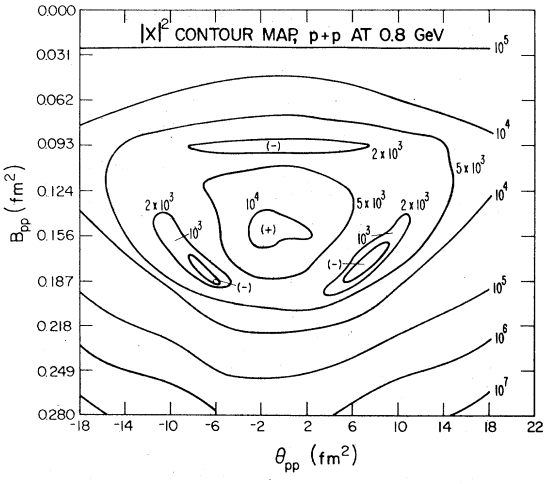

FIG. 1. Contour plot of the total $|\chi|_T^2$ obtained from Eqs. (8) and (9) and the 0.8 GeV $p+p$ cross section and polarization data as a function of B_{pp} and θ_{pp} as discussed in the text. Notice that three discrete solutions are obtained, corresponding to the three minima in $|\chi|_T^2$. The magnitude of $|\chi|_T^2$ is arbitrary.

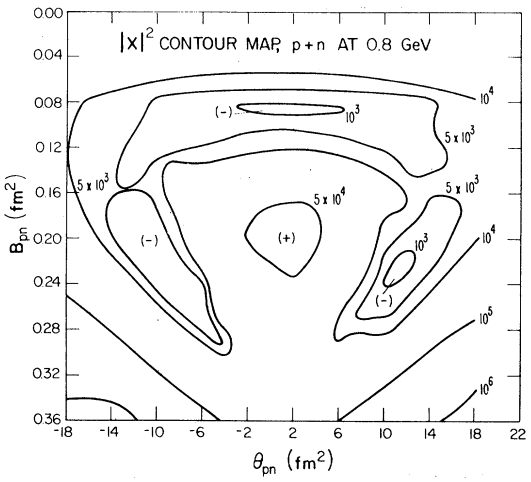

FIG. 2. The same as in Fig. 1 but for $p+n$. Note that three distinct minima in $|\chi|_T^2$ also occur for the $p+n$ system.

630[30] and 1030[31] is well represented by a Gaussian dependence on q for $q\lesssim 3$-4 fm^{-1}. Thus the quantities $\theta_{pj}(\alpha_{spj}-\alpha_{pj})$ and $(B_{spj}+B_{pj})$ are well determined. Two free parameters remain and must be determined by simultaneously optimizing the fit to the cross section and polarization data. The p-n polarization at 800 MeV was estimated by interpolating the very similar $p+n$ polarization data available at 630[30] and 1030 MeV[31]

Shown in Figs. 1 and 2 are cross section and polarization total χ-square values, $|\chi|_T^2$, for $p+p$ and $p+n$ at 0.8 GeV, as a function of B_{pj} and θ_{pj}. Three distinct minima in $|\chi|_T^2$ appear, each of about the same depth for both $p+p$ and $p+n$. The values of $|\chi|_T^2$ shown in Figs. 1 and 2 are arbitrary since the $|\chi|^2$ contribution from the cross section and polarization data have been weighted so that at each minimum, $d\sigma/d\Omega$ and P each account for about one-half of the total $|\chi|_T^2$. The (+) and (−) signs in Figs. 1 and 2 denote local maxima and minima in the $|\chi|_T^2$ contour. The parameter values in Eq. (7) for each of the three $|\chi|_T^2$ minima in Figs. 1 and 2 are given in Table I. The existence of these discrete ambiguities in t_{pj}^{0} and t_{pj}^{s} are generally not appreciated by those who analyze intermediate-energy proton-nucleus data.

The fits to the $p+p$ and $p+n$ cross section (polarization) data using the parameters of solutions 1 and 2 (see Table I) are shown in Fig. 3 (4) as the solid and dashed curves, respectively. The predictions of solution 3 are similar to those of No. 2. The three sets of $p+p$ cross section data indicated by the open boxes, crossed boxes, and solid points are from Refs. 26, 27, and 25, respectively, while the polarization data are from Ref. 28. The

TABLE I. Values of the parameters of the proton-nucleon amplitudes [see Eq. (7)] corresponding to the minima in the total χ^2 for $p+p$ and $p+n$ cross sections and polarizations at 0.8 GeV as discussed in the text.

	Sol. No.	σ^T_{pj} fm^2	α_{pj}	B_{pj} fm^2	θ_{pj} fm^2	α_{spj}	B_{spj} fm^2	$\lvert\chi\rvert_T^2$ Arbitrary units
$p+p$	1	4.73	0.06	0.09	−0.67	−12.2	0.19	1130.0
	2	4.73	0.06	0.17	7.3	1.18	0.11	520.0
	3	4.73	0.06	0.19	−6.0	−1.3	0.09	880.0
$p+n$	1	3.79	−0.2	0.08	1.56	3.8	0.27	850.0
	2	3.79	−0.2	0.23	11.3	0.35	0.12	630.0
	3	3.79	−0.2	0.20	−10.0	−0.82	0.15	1850.0

recent forward angle $p+n$ elastic cross section data are from Carlini,[29] while the remaining cross section data are from Ref. 25 and the $p+n$ polarization data at 630 and 1030 MeV are from Refs. 30 and 31, respectively. In determining the p-n amplitudes only the forward angle cross section data of Carlini[29] were used. Clearly, a more flexible parametrization than that in Eq. (7) would be required to obtain a "perfect" fit to these data.

The question arises as to which, if any, of these sets of solutions will provide fits to the proton-nucleus analyzing power data, $A_y(\theta)$, when used in the KMT optical potential, Eq. (5). To investigate this, calculations were made for $\vec{p}+^{40}$Ca assuming: (a) solutions 1 for both $p+p$ and $p+n$; (b) solutions 2 for both $p+p$ and $p+n$; (c) solutions 3 for both $p+p$ and $p+n$; (d) solutions 1 for $p+p$ and 2 for $p+n$; and (e) the opposite of (d). The results for choices (a) and (b) are shown in Fig. 5 as the solid and dashed curves, respectively. In each

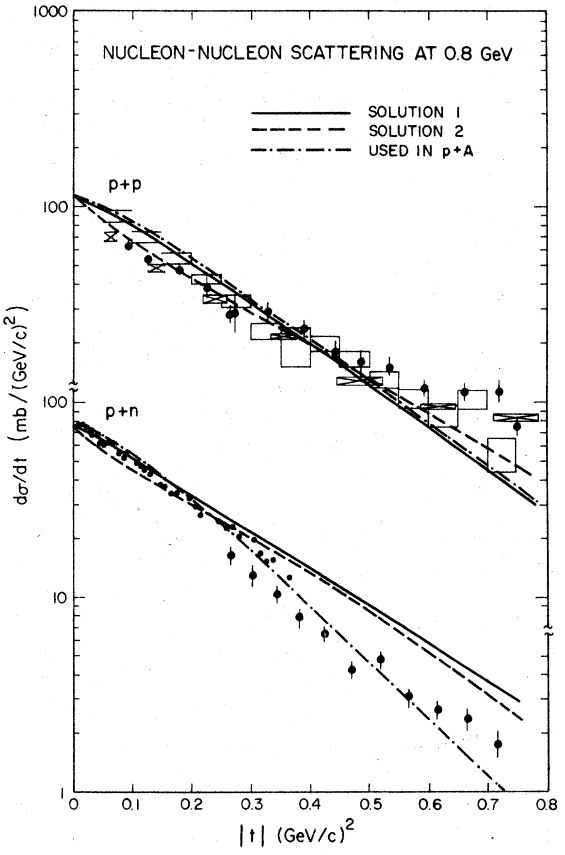

FIG. 3. Fits to the $p+p$ and $p+n$ elastic angular distribution data at 0.8 GeV using Eq. (8) and the parameters (see Table I) of solution 1 (solid curves), solution 2 (dashed curves) and the parameters used in the proton-nucleus calculations which have been adjusted to fit the proton-nucleus analyzing power data (dash-dot curves).

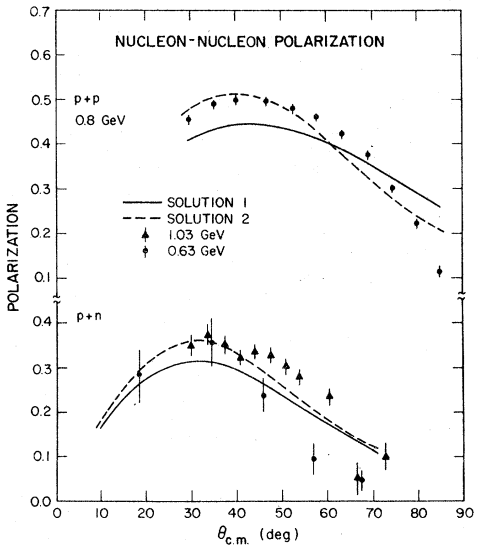

FIG. 4. Fits to the $p+p$ and $p+n$ elastic polarization data using Eq. (9) and parameters corresponding to solutions 1 (solid curves) and 2 (dashed curves) as given in Table I.

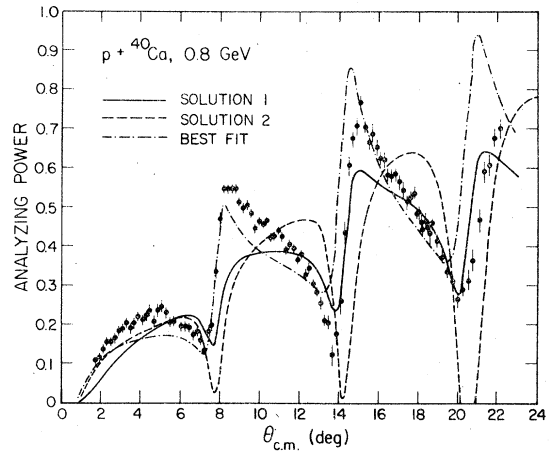

FIG. 5. Predicted elastic analyzing powers for $\vec{p}+{}^{40}Ca$ at 0.8 GeV compared to the data given in Ref. 4. The prediction assuming solution 1 (2) for both the $p+p$ and $p+n$ amplitudes is indicated by the solid (dashed) curve. The dash-dot curve is the best fit obtained by allowing a free variation in the $\bar{\theta}_p$ and $\bar{\alpha}_{sp}$ parameters as discussed in the text.

case good fits to the elastic data were obtained by varying the neutron density geometry. Choice (c) results in a prediction for $A_y(\theta)$ which rises too slowly and drops too rapidly as $\theta_{c.m.}$ increases, resulting in worse agreement with the data than the dashed curve in Fig. 5. Choices (d) and (e) are similar to the dashed curve in Fig. 5. The best results are obtained by assuming solution 1 for both the $p+p$ and $p+n$ amplitudes. Although this prediction is not particularly good, it is encouraging that the overall strength of the analyzing power is correctly predicted. The dash-dot curve in Fig. 5 is a best fit to this $A_y(\theta)$ data starting from the solution 1 amplitudes for $p+p$ and $p+n$, where the only essential variation needed to improve the fit to the data is in the strength of the imaginary part of the spin-orbit potential. The real part, given by the product $(\theta_{pj}\alpha_{spj})$, and the range parameter B_{spj}, are varied only slightly (about 10%) from their values in solution 1. It is certainly possible that the omitted double-spin-flip amplitudes could modify the deduced value for α_{spj} in such a way. Obviously the parameters of solution 1 reproduce the $p+A$ analyzing power fairly well, although some empirical adjustment is needed to obtain a good fit.

Solution 1 is thus preferred, based on the predictions for $A_y(\theta)$. Another way to rate the merits of these several possible N-N amplitudes involves the value deduced for the neutron rms radius which results when the proton-nucleus differential cross section data are fit by varying the neutron density geometry as in Refs. 2–6 with alternate two-nucleon solution sets assumed. Adopting either solution 1 for both the $p+p$ and $p+n$ amplitudes or the empirical result discussed above yields values of Δr_{np} $(\equiv\langle r_n^2\rangle^{1/2}-\langle r_p^2\rangle^{1/2})$ for a wide range of nuclei which are generally in very good agreement with Hartree-Fock predictions.[2-6,11,45] Assuming solutions 2 or 3 for both the $p+p$ and $p+n$ amplitudes would reduce the determined values of Δr_{np} by about 0.2 fm, thus destroying this generally favorable agreement.

The philosophy adopted here is that the proton-nucleus data should be analyzed using N-N amplitudes very similar to the solution 1 values, with variation being allowed to fit the proton-nucleus $A_y(\theta)$ data on a case-by-case basis. Since the real and especially the imaginary strengths of the $p+A$ spin-orbit potential are to be freely searched, $t^s_{pp}(q^2)$ and $t^s_{pn}(q^2)$ have been replaced by an average amplitude $\bar{t}^s_p(q^2)$ with corresponding parameters $\bar{\theta}_p$, $\bar{\alpha}_{sp}$, and $\bar{B}_{sp}$.[2] The value of $\bar{B}_{sp}$ is fixed equal to 0.2 fm^2, this being the average of B_{spp} and B_{spn} for solution 1. The strength of the real part of the spin-orbit potential, which is proportional to $(\bar{\theta}_p\bar{\alpha}_{sp})$ is allowed to vary but always remains within ~10% of the isospin average of the products $(\theta_{pp}\alpha_{spp})$ and $(\theta_{pn}\alpha_{spn})$ of solution No. 1. The individual values of $\bar{\theta}_p$ and $\bar{\alpha}_{sp}$ which give the best fits to the various $A_y(\theta)$ data considered here will be given later.

Varying the N-N spin parameters alters the fits to the N-N cross section and polarization data. Since the primary concern here is to fit $p+A$ angular distributions, one should not make changes in nucleon-nucleon parameters which destroy the fit to the N-N elastic cross sections, for otherwise one has abandoned the microscopic approach for a phenomenological one. Thus, one should in general recover the fit to the N-N elastic cross section. This is most readily accomplished by varying B_{pj} but as it turns out no variation in B_{pp} is required and only a small variation (compared to the fitting uncertainty[5,6]) in B_{pn}, from 0.08 to 0.12 fm^2, is needed.[2-6] Most of the increase in B_{pn} is needed to produce a better fit to the two sets of $p+n$ cross section data.[25,29] Thus the spin-independent parameters used in this analysis are $\sigma^T_{pp}=4.73$ fm^2, $\alpha_{pp}=0.06$, $B_{pp}=0.09$ fm^2, $\sigma^T_{pn}=3.79$ fm^2, $\alpha_{pn}=-0.2$, and $B_{pn}=0.12$ fm^2. The average of the values of $\bar{\theta}_p$ and $\bar{\alpha}_{sp}$ determined for the seven cases studied here (see Sec. III) are 9.2 fm^2 and 0.68, respectively, while $\bar{B}_{sp}=0.2$ fm^2 always. The predictions for the $p+p$ and $p+n$ elastic cross sections based on these parameters are indicated by the dash-dot curves in Fig. 3. The maximum variation in B_{pj} allowed by the statistical error in the data is considered later in estimating the error in the deduced neutron radius.[5,6]

The main points of this subsection can now be

given. First of all, the various solutions for the N-N spin-independent and spin-orbit amplitudes [t^0_{pj} and t^s_{pj} in Eq. (6)] are not necessarily claimed to accurately represent reality. Only a complete analysis of the full set of N-N experiments[24,41] can achieve this. Secondly, the occurrence of the discrete ambiguities seen in Figs. 1 and 2 and the possible importance of double-spin-flip amplitudes as suggested by the recent Argonne data[42,43] should serve to caution analysts against making premature assumptions about the most important, spin-independent N-N amplitudes. Finally, although the solution 1 N-N amplitudes used here and elsewhere[1-16,44,45] result in Δr_{np} values which are generally in good agreement with Hartree-Fock predictions,[2-6,11,45] one must for the time being place higher confidence in the determination of the relative differences between neutron densities and radii than in their absolute values. Again, based on the analyzing power predictions in Fig. 5 and the Δr_{np} results of numerous analyses,[4,7,11,13,45,46] there may not be any serious problem with the N-N amplitudes generally chosen.[1-16,44,45] However, because of the questions raised here, relative differences of neutron densities will receive the greater emphasis throughout this article.

B. Extraction of the proton density from empirical charge densities

Customarily the point proton density distribution is extracted from empirical charge densities with only the proton electric form factor being considered.[1-16] Thus in this simple approximation

$$\rho_p(r) \cong \mathfrak{F}^{-1}\{\tilde{\rho}_{ch}(q^2)/G_E^P(q^2)\}, \tag{10}$$

where $\tilde{\rho}_{ch}$ is the momentum-transfer-space representation of the charge density, G_E^P is the electric form factor of the proton[47] and $\mathfrak{F}^{-1}\{\}$ indicates an inverse Fourier transform operation. Bertozzi *et al.*[20] have however shown that the neutron's electric form factor contributes to the total measured charge density and for nuclei with partially filled l shells the magnetic form factors[47] of both the proton and the neutron also contribute to $\tilde{\rho}_{ch}$. Generally such corrections to $\rho_p(r)$ are rather small and have usually been ignored in proton-nucleus calculations. However, as will be shown, these corrections are of about the same size as the second-order correlation terms of the optical potential and tend to *cancel* their effects on the values deduced for neutron matter radii. For some nuclei this cancellation is complete. Because of the desire to obtain relative differences in neutron densities as accurately as possible, and owing to the fact that these electromagnetic corrections are isotopically dependent, it is important that such corrections be properly taken into account.

The expression relating the various nucleon form factors to the charge density is derived in detail in Ref. 20 and will not be repeated here. In general the nuclear charge form factor, $\tilde{\rho}_{ch}(q^2)$, for spherically symmetric densities is

$$\tilde{\rho}_{ch}(q^2) = 4\pi\left[\tilde{G}_E^P(q^2)\int_0^\infty x^2 j_0(qx)\rho_p(x)dx + \tilde{G}_E^N(q^2)\int_0^\infty x^2 j_0(qx)\rho_n(x)dx \right.$$
$$\left. -(q^2/4M^2)\sum_{\substack{i=\text{unfilled}\\ l\text{ shells}}}[2G_M^i(q^2)-\tilde{G}_E^i(q^2)](j_i^2 - l_i^2 - s_i^2)\int_0^\infty \frac{j_1(qx_i)}{(qx_i)}\rho_{nlj}(x_i)x_i^2 dx_i\right], \tag{11}$$

where terms to order M^{-2} are kept (M is the nucleon mass). In this expression the electric form factors are corrected for relativistic effects by the Darwin-Foldy factor, where

$$\tilde{G}_E^i(q^2) = (1 - q^2/8M^2)G_E^i(q^2), \tag{12}$$

$G_E^i(q^2)$ being the experimentally determined form factor.[47] The proton and neutron densities are $\rho_p(x)$ and $\rho_n(x)$, respectively. In the last term of Eq. (11), the sum includes all neutrons and protons in partially filled l shells. Those in filled l shells are not summed since in j-j coupling the spin-orbit contributions from such nucleons add to zero, at least in first order. The quantities j_i^2, l_i^2, and s_i^2 are the eigenvalues of the squares of the total, orbital and spin angular momentum operators for the ith nucleon. The density $\rho_{nlj}(x_i)$ is the single nucleon density for the (nlj) shell model level for the ith nucleon. For example in ^{48}Ca the eight neutrons in the $1f_{7/2}$ level and in ^{208}Pb the 12 protons in the $1h_{11/2}$ and the 14 neutrons in the $1i_{13/2}$ levels would be included. In all there are four corrections to Eq. (10) to be considered here. The point proton density may be evaluated by solving Eq. (11) for $\rho_p(x)$. The result is

$$\rho_p(x) = \frac{1}{2\pi^2}\int_0^{q_{max}} j_0(qx)\frac{[\tilde{\rho}_{ch}(q^2) - \tilde{\rho}_n^{(1)}(q^2) - \tilde{\rho}_{so}^{(1)}(q^2)]}{\tilde{G}_E^P(q^2)}q^2 dq, \tag{13}$$

where

$$\tilde{\rho}_{ch}(q^2) = 4\pi \int_0^\infty x^2 j_0(qx)\rho_{ch}(x)dx \,, \tag{14a}$$

$$\tilde{\rho}_n^{(1)}(q^2) = 4\pi \tilde{G}_E^N(q^2) \int_0^\infty x^2 j_0(qx)\rho_n(x)dx \,, \tag{14b}$$

$$\tilde{\rho}_{so}^{(1)}(q^2) = -(\pi q^2/M^2)\sum_i [2G_M^i(q^2) - \tilde{G}_E^i(q^2)](j_i^2 - l_i^2 - s_i^2) \int_0^\infty \frac{j_1(qx_i)}{(qx_i)} \rho_{nlj}(x_i)x_i^2 dx_i \,. \tag{14c}$$

The densities ρ_{ch}, ρ_n, ρ_p, and ρ_{nlj} are normalized to Z, N, Z, and 1, respectively.

The neutron density $\rho_n(r)$, in Eq. (14b) used to evaluate the point proton density is itself to be determined from the proton scattering analysis. Thus one should in general iterate until self-consistency is achieved. In practice only one iteration is required provided that a reasonable estimate for the final $\rho_n(r)$ is used initially. In this analysis, neutron densities obtained from the first order analyses have been used in Eq. (14b). Typically these electromagnetic corrections cause the neutron matter radius to decrease from the first order results by ~0.01 to 0.03 fm. Using these new neutron densities in Eq. (13) for a second iteration changes the resulting proton radius by less than 5×10^{-5} fm.

For the bound state densities, $\rho_{nlj}(x_i)$, simple eigenstates of Woods-Saxon potentials have been used. The binding potential parameters in the usual notation[48] V_{s0}, r_0, a_0, r_{s0}, a_{s0}, and r_c are given by 6.0 MeV, 1.2, 0.65, 1.2, 0.65, and 1.2 fm, respectively. The real well depth was adjusted to give the correct single particle binding energy in each case. The momentum transfer integration cutoff, q_{max} in Eq. (13), has the value of the maximum momentum transfer of the electron scattering data.[49-54] Finally, the empirical charge densities used in Eq. (14a) have been obtained from the literature.[49-54]

In Table II the effects of each of the just discussed corrections on the proton matter radius have been calculated for a number of nuclei. The values given in this table are the changes in the rms radius of the proton density which result when each of the various corrections is included. Generally the correction due to G_E^N adds about 0.02 fm to the proton radius, the Darwin-Foldy factor subtracts 0.005 fm, the G_M^N correction adds to $\langle r_p^2\rangle^{1/2}$ while G_M^P subtracts from $\langle r_p^2\rangle^{1/2}$. The net correction to $\langle r_p^2\rangle^{1/2}$ varies from increases of 0.006 to 0.034 fm. When these corrections are included in the proton-nucleus calculations and the fit to the proton elastic angular distribution is recovered by varying the neutron geometry, the neutron rms radius, $\langle r_n^2\rangle^{1/2}$ *decreases* by about Z/N times the amount of increase of $\langle r_p^2\rangle^{1/2}$ given in Table II. Hence Δr_{np} *decreases* owing to these electromagnetic corrections by amounts varying from 0.01 to 0.06 fm, which are comparable to and in the opposite direction from the effects produced on Δr_{np} by target nucleon correlation terms.[11] Therefore, it is inconsistent to include correlations in one's calculations without also including these electromagnetic corrections to the proton density. For several nuclei (^{48}Ca, ^{124}Sn, and ^{208}Pb) it turns out that the simple first-order result for

TABLE II. Changes in the rms radius of the point proton density due to the various electromagnetic corrections discussed in the text. All values are in Fermis.

Correction	Nucleus ^{40}Ca	^{48}Ca	^{58}Ni	^{64}Ni	^{116}Sn	^{124}Sn	^{208}Pb
G_E^N	0.017	0.024	0.017	0.020	0.017	0.020	0.017
Darwin – Foldy	−0.005	−0.005	−0.004	−0.005	−0.004	−0.004	−0.003
G_M^N		0.015	0.010	0.003	0.001	0.004	0.007
G_M^P			−0.011	−0.010	−0.008	−0.009	−0.006
Total	0.012	0.034	0.012	0.008	0.006	0.011	0.015

Δr_{np} [2,4,5] is much closer to the result of a full calculation, which includes second-order correlations *and* these electromagnetic corrections, than results of second-order calculations which include correlations only.

C. Approximate treatment of the second-order optical potential terms

Historically, target-nucleon correlation corrections to proton-nucleus scattering calculations have been of considerable interest to theorists.[7-12,17-19,40,55-57] Many of these second-order calculations were applied to proton scattering from ^{4}He.[18,19,40,56,57] Recently, calculations by Boridy and Feshbach,[9] Varma and collaborators,[8] Schaeffer and his collaborators,[10,11] and Alkhazov[12] have studied correlation effects in large nuclei ($A \geq 40$) using a variety of methods. These numerous calculations are consistent with one another in demonstrating that these effects are fairly small for large nuclei and cause the diffractive maxima to be increased generally by 10–30%, the amount increasing for larger scattering angles.[8-12] From these calculations it appears quite unlikely that information concerning two-body correlations can be extracted from analyses of proton-nucleus scattering data. However, reasonable estimates of these effects should be included in analyses attempting to determine neutron densities accurately.

Within the framework of KMT, Feshbach *et al.*[18,19] have treated the inherently nonlocal second- and third-order optical potentials by using a factorization approximation and an eikonal assumption and have solved coupled equations to obtain elastic scattering cross sections. This numerically difficult method has generally been applied to the simplest case, of $p+^4$He, where such second-order effects are fairly large.[18,19,40] However, since correlation effects are small in heavy nuclei, a perturbation treatment of these terms should suffice. Such an approach has been independently developed by Harrington and Varma[8] and by Layly and Schaeffer.[10]

The approach adopted here, within the KMT formalism, for estimating the Pauli and short-range dynamical correlation corrections is similar to that of Harrington and Varma,[8] who use the Glauber and local density approximations to obtain local forms for the second-order optical potential which depend on $\sim\rho^2$. The same eikonal and local density approximations are made by Layly and Schaeffer,[10] within the KMT formalism, to obtain other similar, local $\sim\rho^2$ forms for the second-order optical potential. Their estimates for the center-of-mass transformation correction will be used.[10,11]

It should be emphasized that all calculations of the corrections to proton-nucleus scattering due to target nucleon correlations make use of the eikonal approximation, whether they work in the KMT[9-11,17-19,40] or in the Glauber formalisms.[7,8,12,55-57] In following Harrington and Varma,[8] the Glauber approach is being used only to obtain an approximation for the second-order KMT optical potential term in Eq. (5). The proton-nucleus scattering amplitude is still calculated from an optical potential via solution of the Schrödinger equation with *no* additional eikonal approximations being made.

The derivation of the expressions for the second-order optical potentials of Harrington and Varma is given in detail in Ref. 8 and will only be outlined here. In Glauber theory the nucleon-nucleus scattering amplitude is written as[8,23]

$$F(q) = -\frac{k}{2\pi i}\int d^2b\, e^{-i\vec{q}\cdot\vec{b}}\,\Gamma(\vec{b})\,, \tag{15}$$

where $\vec{q}=\vec{k}_f-\vec{k}_i$, $\vec{b}$ is the impact parameter, and

$$\Gamma(\vec{b}) = 1-\langle\Psi|\prod_{i=1}^{A}[1-\gamma(\vec{b}-\vec{b}_i)]|\Psi\rangle\,. \tag{16}$$

In this expression $|\Psi\rangle$ is the nuclear ground-state wave function, $\vec{b}_i$ is the component of $\vec{r}_i$, the position of the ith target nucleon in the plane perpendicular to the incident proton, and $\gamma(\vec{b})$ is a two-dimensional transform of the nucleon-nucleon scattering amplitude, $f(q^2)$, given by

$$\gamma(\vec{b}) = \frac{1}{2\pi i k_0}\int d^2q\, e^{i\vec{q}\cdot\vec{b}} f(q^2)\,. \tag{17}$$

Expanding the second term in Eq. (16) to second order in the density using the correlation expansion for the nuclear density,[58] Harrington and Varma obtain

$$\Gamma(b) \cong \Gamma_0(b)+\Gamma_2(b)+\cdots\,, \tag{18}$$

where

$$\Gamma_0(b) = 1-(1-\langle\gamma\rangle)^A\,, \tag{19}$$

$$\Gamma_2(b) = -\tfrac{1}{2}A(A-1)(1-\langle\gamma\rangle)^{A-2}(\langle\gamma_1\gamma_2\rangle-\langle\gamma\rangle^2)\,. \tag{20}$$

In these expressions

$$\langle\gamma\rangle = \int d^3r_1\rho_1(\vec{r}_1)\gamma(\vec{b}-\vec{b}_1)\,, \tag{21}$$

$$\langle\gamma_1\gamma_2\rangle = \int d^3r_1 d^3r_2\rho_2(\vec{r}_1,\vec{r}_2)\gamma(\vec{b}-\vec{b}_1)\gamma(\vec{b}-\vec{b}_2)\,, \tag{22}$$

and the densities ρ_1 and ρ_2 are the one- and two-body densities given by

$$\rho_2(\vec{r}_1,\vec{r}_2)=\int d^3r_3\cdots d^3r_A\delta^3\left(A^{-1}\sum_i\vec{r}_1\right)\times\rho_{\rm int}(\vec{r}_1,\cdots,\vec{r}_A)\,, \tag{23}$$

$$\rho_1(\vec{r}_1)=\int d^3r_2\rho_2(\vec{r}_1,\vec{r}_2)\,. \tag{24}$$

In Eq. (23) the internal density $\rho_{\rm int}$ which depends only on relative coordinates is introduced and the center-of-mass constraint imposed. This one body density satisfies $\int d^3r_1\rho_1(\vec{r}_1)=1$. The quantity $[\langle\gamma_1\gamma_2\rangle-\langle\gamma\rangle^2]$ is given by

$$\langle\gamma_1\gamma_2\rangle-\langle\gamma\rangle^2=\int d^3r_1d^3r_2C_2(\vec{r}_1,\vec{r}_2)\gamma(\vec{b}-\vec{b}_1)\gamma(\vec{b}-\vec{b}_2)\,, \tag{25}$$

where $C_2(\vec{r}_1,\vec{r}_2)=\rho_2(\vec{r}_1,\vec{r}_2)-\rho_1(\vec{r}_1)\rho_1(\vec{r}_2)$, is the two-body correlation function. The second-order eikonal phase shifts,[23] $\delta^{(2)}$, are then defined by setting

$$\Gamma_2(b)=-\tfrac{1}{2}A(A-1)(1-\langle\gamma\rangle)^{A-2}\delta^{(2)}(b)\,. \tag{26}$$

The two-body correlation functions assumed for the Pauli and short-range dynamical correlations (SRD) are those of Boridy and Feshbach[9] who define

$$C_2(\vec{r}_1,\vec{r}_2)\cong\rho_1(\vec{r}_1)\rho_1(\vec{r}_2)\times[f_{\rm Pauli}(|\vec{r}_1-\vec{r}_2|)+f_{\rm SRD}(|\vec{r}_1-\vec{r}_2|)+f_{\rm Pauli}(|\vec{r}_1-\vec{r}_2|)f_{\rm SRD}(|\vec{r}_1-\vec{r}_2|)]\,. \tag{27}$$

For a noninteracting Fermi gas the Pauli correlation function for a nucleus with A nucleons is[9,59]

$$f_{\rm Pauli}(x)=-\frac{9}{4}\frac{A-4}{A-1}\left[\frac{j_1(k_Fx)}{(k_Fx)}\right]^2, \tag{28}$$

where k_F is the local Fermi momentum, here assumed to be position dependent according to[8]

$$k_F(r)=[1.5\pi^2A\rho_1(r)]^{1/3}\,. \tag{29}$$

The presumed short-range repulsion between nucleons[60] results in a dynamical correlation which prevents the centers of two nucleons from being within ~0.5 fm of each other. The form adopted by Boridy and Feshbach[9] and Varma[8] for this short-range dynamical correlation is

$$f_{\rm SRD}(x)=-\exp(-x^2/b^2)\,, \tag{30}$$

where $b=0.4$ fm. To enable the integrations in Eq. (25) to be carried out analytically, $f_{\rm Pauli}(x)$ in Eq. (28) must be approximated by a Gaussian or[8]

$$f_{\rm Pauli}(x)\cong-\tfrac{3}{10}(\pi/5)^{1/2}[(A-4)/(A-1)]\times\exp(-k_F^2x^2/5)\,. \tag{31}$$

This approximation will be tested later. By assuming the forms in Eqs. (30) and (31) and by taking Gaussian forms for the scattering amplitudes in Eq. (17) the six-dimensional integral in Eq. (25) can be reduced to a one-dimensional integral along the Z axis (incident beam direction) provided that the ranges of the correlation functions and interactions, $\gamma(b)$, are small compared to distances over which the nuclear density changes. This should be a reasonable approximation for large nuclei since these ranges are typically ~1 fm. With these approximations $[\rho_1(\vec{r}_1)\rho_1(\vec{r}_2)]$ in Eq. (27) can be replaced with $\rho_1^2((\vec{r}_1+\vec{r}_2)/2)$ and can be removed from all but the last integral over Z. For example, the $f_{\rm Pauli}(x)$ term in Eq. (27) yields[8]

$$\delta^{(2)}_{\rm Pauli}(b)=-\left[\frac{A-4}{A-1}\right]\left[\frac{\hat{\sigma}}{2}\right]^2\int_{-\infty}^{\infty}\frac{dZ\rho_1^2(b,Z)3\pi}{[10k_F(r)][1+8Bk_F^2(r)/5]}\,, \tag{32}$$

using Eqs. (20), (25), (26), (27), (29), and (31) where

$$\hat{\sigma}=\bar{\sigma}^T(1-i\bar{\alpha})\,, \tag{33}$$

and

$$\bar{\sigma}^T=\frac{Z}{A}\sigma_{pp}^T+\frac{N}{A}\sigma_{pn}^T\,, \tag{34}$$

$$\bar{\alpha}=\frac{Z\sigma_{pp}^T\alpha_{pp}+N\sigma_{pn}^T\alpha_{pn}}{Z\sigma_{pp}^T+N\sigma_{pn}^T}\,, \tag{35}$$

and

$$B=\frac{Z}{A}B_{pp}+\frac{N}{A}B_{pn}\,. \tag{36}$$

The results for the second-order eikonal phase shifts can be related directly to a second-order optical potential, beginning with the relation[8]

$$[A/(A-1)]\{1-\exp[i\hat{\chi}_{\rm opt}(b)]\}=\Gamma(b)\,, \tag{37}$$

so that as before

$$F(q)=-\frac{k}{2\pi i}\frac{A}{A-1}\int d^2b\,e^{-i\vec{q}\cdot\vec{b}}\{1-\exp[i\hat{\chi}_{\rm opt}(b)]\}\,. \tag{38}$$

Expanding $\hat{\chi}_{\rm opt}$ in powers of $\langle\gamma\rangle$ one obtains to second order in the density, with $\hat{\chi}_{\rm opt}=\hat{\chi}_1+\hat{\chi}_2+\cdots$,

$$i\hat{\chi}_1(b)=-(A-1)\langle\gamma\rangle\,, \tag{39}$$

$$i\hat{\chi}_2(b)=\tfrac{1}{2}(A-1)^2(\langle\gamma_1\gamma_2\rangle-\langle\gamma\rangle^2)=\tfrac{1}{2}(A-1)^2\delta^{(2)}(b)\,, \tag{40}$$

and finally using the relation[8,23]

$$\hat{\chi}_{\rm opt}(b)=-\frac{\mu c^2}{\hbar^2c^2k_N}\int_{-\infty}^{\infty}dZ\,U_{\rm KMT}^{\rm opt}(r)\,, \tag{41}$$

an eikonal estimate of the second-order optical potential $U^{(2)\text{opt}}(r)$ due to the first term in Eq. (27) is obtained as

$$U^{(2)\text{opt}}_{\text{Pauli}}(r) \cong -\frac{i(\hbar c)^2 k_N}{2\mu c^2}(A-1)(A-4)(\hat{\sigma}/2)^2 \rho_1^2(r) \times\{3\pi/[10k_F(r)]\}[1+8B\,k_F^2(r)/5]^{-1}. \quad (42)$$

In Eqs. (41) and (42) relativistic kinematics are assumed, so that k_N is taken to be the relativistic center-of-momentum system wave number and (μc^2) is interpreted as the reduced energy,[39] $\epsilon_1\epsilon_2/(\epsilon_1+\epsilon_2)$, ϵ_i being the total relativistic energy of either the incident proton or target nucleus in the proton-nucleus center-of-momentum system. As a reminder to the reader, $\rho_1(r)$ in Eq. (42) is the total matter density, normalized such that $\int d^3r \rho_1(r) = 1$.

In a similar fashion the second-order potential due to the short-range dynamical correlations, Eq. (30) is found to be

$$U^{(2)\text{opt}}_{\text{SRD}}(r) \cong -\frac{i(\hbar c)^2 k_N}{2\mu c^2}(A-1)^2(\hat{\sigma}/2)^2\sqrt{\pi}\rho_1^2(r)\frac{b^3}{b^2+8B}, \quad (43)$$

and the Pauli and short-range interference term in Eq. (27) yields the potential,

$$U^{(2)\text{opt}}_{\text{PSR-I}}(r) \cong \frac{i(\hbar c)^2 k_N}{2\mu c^2}(A-1)(A-4)(\hat{\sigma}/2)^2 \times(3\pi/10)\rho_1^2(r)[k_F^2(r)+5b^{-2}]^{-1/2} \times\{1+8B[k_F^2(r)/5+b^{-2}]\}^{-1}. \quad (44)$$

To reiterate, the approximations or assumptions made in obtaining these local $\sim\rho^2$ estimates of contributions to the second-order optical potential are: (1) the eikonal approximation; (2) the local-density approximation; (3) further approximation of the two-nucleon scattering amplitudes and correlation functions with Gaussian forms; and (4) the assumption that the ranges of the $N-N$ interaction and correlation lengths are small compared to the nuclear radius. The eikonal approximation for second-order terms is common both to Glauber and KMT treatments[9-11,17-19,40] and the short-range assumptions should be valid since only large nuclei with radii from 3–5 fm are considered here. The Gaussian approximation, Eq. (31), for the Pauli correlation function, Eq. (28), has been tested by using a sum of Gaussians which better approximates Eq. (28) than Eq. (31) does. The resultant effect on the predicted proton-nucleus angular distribution is negligibly different from that predicted by Eq. (42).

Layly and Schaeffer[10] have shown that the second-order potential can be in general reduced to a simple local form by making the eikonal approximation in the propagator and also a local density approximation. The result is

$$U^{(2)}(q) \cong i(A-1)^2\frac{\mu c^2}{(\hbar c)^2 k_N}t^2(q/2)l_c \times\int e^{-i\vec{q}\cdot\vec{r}'}\rho_1^2(\vec{r}')d^3r', \quad (45)$$

where t is the $N-N$ t matrix and l_c is an effective "correlation length." This form will be used to estimate the center-of-mass transformation correction.

If shell model or Hartree-Fock wave functions are to be used then the spurious center-of-mass motion[18,38] inherent in such densities must first be removed before using these densities in the optical model calculations. For instance, with antisymmetrized harmonic oscillator wave functions the correction factor $\exp(q^2R^2/4A)$ [8] multiplies the uncorrected proton-nucleus scattering amplitude to yield the final cross section. For large nuclei this harmonic oscillator form is unrealistic, and it overestimates the spurious center-of-mass motion correction at large momentum transfers. Harrington and Varma[8] and Alkhazov[12] have developed a better approximation for this correction, applicable for large nuclei. However, when charge densities deduced from electron scattering (see Sec. II B) and similar one-body neutron densities are used as input into the optical potential calculation no such correction is needed. The transformation from the nuclear center-of-mass to the proton-nucleus center-of-mass system does, however, need to be taken into account. Such reference-frame-transformation corrections have been estimated by Chaumeaux *et al.*[11] For this correction only, the effective correlation length in Eq. (45) (from Ref. 11) is

$$l_{\text{c.m.}} = (R_{\text{c.m.}}/A)(1-q^2\langle r^2\rangle/12), \quad (46)$$

where $R_{\text{c.m.}} = \sqrt{\pi}ac$, a and c being the diffuseness and radius of a Fermi matter density, and $\langle r^2\rangle$ is the mean square matter radius.

The correction potential in coordinate space is

$$U^{(2)\text{opt}}_{\text{c.m.}}(r) = (2\pi)^{-3}\int e^{i\vec{q}\cdot\vec{r}}U^{(2)}(q)d^3q. \quad (47)$$

Assuming

$$t^2(q/2) = -(\hat{\sigma}/2)^2\left[\frac{(\hbar c)^2 k_N}{\mu c^2}\right]^2\exp(-Bq^2/2), \quad (48)$$

one gets

$$U^{(2)\mathrm{opt}}_{\mathrm{c.m.}}(r) \cong -\frac{i(A-1)^2}{(2\pi)^3}\frac{(\hbar c)^2 k_N}{\mu c^2}(\hat{\sigma}/2)^2(R_{\mathrm{c.m.}}/A)\iint e^{i\vec{q}\cdot(\vec{r}-\vec{r}')}e^{-Bq^2/2}(1-q^2\langle r^2\rangle/12)\rho_1^{\,2}(r')d^3r'd^3q\,. \tag{49}$$

The calculations of Chaumeaux *et al.*[11] reveal that this correction is small, even compared to the small Pauli correlation correction for the large nuclei ($A \geq 40$) to be considered here. Hence a further simplification is justifiable, namely that $l_{\mathrm{c.m.}} \cong R_{\mathrm{c.m.}}/A$. Assuming as above that the range of t in Eq. (48) is small compared to the nuclear size, the final expression for $U^{(2)\mathrm{opt}}_{\mathrm{c.m.}}(r)$ becomes

$$U^{(2)\mathrm{opt}}_{\mathrm{c.m.}}(r) \cong -i(A-1)^2\left[\frac{(\hbar c)^2 k_N}{\mu c^2}\right]\left(\frac{\hat{\sigma}}{2}\right)^2\frac{R_{\mathrm{c.m.}}}{A}\rho_1^{\,2}(r)\,, \tag{50}$$

where $\int \rho_1(r)d^3r = 1$. Note that unlike the previous correction potentials in Eqs. (42), (43), and (44) this center-of-mass correction depends roughly on A^{-1} and so, as one would expect, becomes much less important in comparison to the other correlation corrections for larger nuclei.

In all of the above calculations, the spin dependence of the $N-N$ amplitude has been neglected. After the central term, the next largest part of the proton-nucleus optical potential is the spin-orbit part[2-6] and hence the largest correction to this potential, that due to Pauli correlations, should be evaluated. This will be done by generalizing the derivation of Harrington and Varma.[8]

As in Sec. IIA the $N-N$ amplitude is written as $f_{pj}(q^2) = t^0_{pj}(q^2) + it^s_{pj}(q^2)(\vec{\sigma}_p + \vec{\sigma}_j)\cdot\hat{n}$ and generalizing Eq. (17) obviously yields

$$\bar{\gamma}_s(\vec{b}) = \frac{1}{2\pi i k_0}\int d^2q e^{i\vec{q}\cdot\vec{b}}[\bar{t}^0_p(q^2) + i\bar{t}^s_p(q^2)(\vec{\sigma}_p + \vec{\sigma}_j)\cdot\hat{n}]\,, \quad \bar{\gamma}_s(\vec{b}) = \gamma_0(\vec{b}) + \gamma_s(\vec{b})(\vec{\sigma}_p\cdot\hat{n}) + \gamma_s(\vec{b})(\vec{\sigma}_j\cdot\hat{n})\,, \tag{51}$$

where $\gamma_0(\vec{b})$ is identical to the $\gamma(\vec{b})$ in Eq. (17) and $\bar{t}^0_p(q^2)$ is the average of t^0_{pp} and t^0_{pn} as in Eqs. (34)–(36). From Eqs. (20, (25), (26), (27), (29), and (31), the Pauli phase shift $\delta^{(2)}_{\mathrm{Pauli}}(\vec{b})$ becomes

$$\delta^{(2)}_{\mathrm{Pauli}}(\vec{b}) = \iint d^3r_1 d^3r_2 \bar{\gamma}_s(\vec{b}-\vec{b}_1)\bar{\gamma}_s(\vec{b}-\vec{b}_2)\rho_1(\vec{r}_1)\rho_1(\vec{r}_2)f_{\mathrm{Pauli}}(|\vec{r}_1-\vec{r}_2|)\,. \tag{52}$$

From the last two expressions nine terms for $\delta^{(2)}_{\mathrm{Pauli}}(\vec{b})$ are obtained. If the restriction to spin 0 target nuclei is made and if the generally nonvanishing contributions of the m, g, and h $N-N$ amplitudes [see Eq. (6)] are neglected then

$$\begin{aligned}\delta^{(2)}_{\mathrm{Pauli}}(\vec{b}) = \iint\, & d^3r_1 d^3r_2 \rho_1(\vec{r}_1)\rho_1(\vec{r}_2)f_{\mathrm{Pauli}}(|\vec{r}_1-\vec{r}_2|) \\ & \times\{\gamma_0(\vec{b}-\vec{b}_1)\gamma_0(\vec{b}-\vec{b}_2) + 2\gamma_0(\vec{b}-\vec{b}_1)\gamma_s(\vec{b}-\vec{b}_2)(\vec{\sigma}_p\cdot\hat{n}) + \gamma_s(\vec{b}-\vec{b}_1)\gamma_s(\vec{b}-\vec{b}_2)[(\vec{\sigma}_p\cdot\hat{n})(\vec{\sigma}_p\cdot\hat{n}) + (\vec{\sigma}_1\cdot\hat{n})(\vec{\sigma}_2\cdot\hat{n})]\}\,,\end{aligned} \tag{53}$$

where symmetry of the integral with respect to the interchange of labels 1 and 2 is used. So to lowest order in the spin amplitudes,

$$\delta^{(2)}_{\mathrm{Pauli}}(\vec{b}) \cong \iint d^3r_1 d^3r_2 \rho_1(\vec{r}_1)\rho_1(\vec{r}_2)f_{\mathrm{Pauli}}(|\vec{r}_1-\vec{r}_2|)[\gamma_0(\vec{b}-\vec{b}_1)\gamma_0(\vec{b}-\vec{b}_2) + 2\gamma_0(\vec{b}-\vec{b}_1)\gamma_s(\vec{b}-\vec{b}_2)(\vec{\sigma}_p\cdot\hat{n})]\,, \tag{54}$$

where the first term yields Eq. (42) and the second term results in the leading Pauli correlation correction to the spin-orbit potential. Assuming the parametrization in Eq. (7)

$$\gamma_s(\vec{b}) = \frac{i\hat{\theta}\hbar c}{16\pi^2 Mc^2}\int d^2q e^{i\vec{q}\cdot\vec{b}}|q|\exp(-\bar{B}_{sp}q^2)\,, \tag{55}$$

where $\hat{\theta} = \bar{\theta}_p(1 - i\bar{\alpha}_{sp})$. Now taking $f_{\mathrm{Pauli}}(x)$ from Eq. (31) and again using short range and local density approximations, the Pauli correlation correction to the proton-nucleus spin-orbit optical potential is

$$\begin{aligned}U^{(2)\mathrm{opt}}_{\mathrm{Pauli,S.O.}}(r) \cong & -i(A-1)(A-4)(3\pi/1280)\left[\frac{(\hbar c)^3\hat{\theta}\hat{\sigma}}{\mu c^2 \bar{B}_{sp} BMc^2}\right] \\ & \times\rho_1(r)\frac{1}{r}\frac{d}{dr}\left[\frac{\rho_1(r)}{k_F(r)\{[1/4B + k_F^{\,2}(r)/5][1/4\bar{B}_{sp} + k_F^{\,2}(r)/5] - k_F^{\,4}(r)/25\}}\right](\vec{\sigma}\cdot\vec{l})\,.\end{aligned} \tag{56}$$

Thus the final, complete optical potential used in the calculations reported here is

$$U^{(1+2)\mathrm{opt}}(r) = U^{(1)}(r) + U^{(2)\mathrm{opt}}_{\mathrm{Pauli}}(r) + U^{(2)\mathrm{opt}}_{\mathrm{SRD}}(r) + U^{(2)\mathrm{opt}}_{\mathrm{PSR\text{-}I}}(r) + U^{(2)\mathrm{opt}}_{\mathrm{c.m.}}(r) + U^{(2)\mathrm{opt}}_{\mathrm{Pauli,S.O.}}(r)\,, \tag{57}$$

where $U^{(1)}(r)$ is the usual first-order, spin-dependent KMT optical potential shown in detail in Ref. 61, and is basically of the $(A-1)t(q^2)\bar{\rho}(q^2)$ form.[6]

The largest of these small second-order correction terms is that due to Pauli correlations.[7-12] The general effect that these terms have on the proton-nucleus angular distribution is to shift the diffractive maxima upward, thus decreasing the overall slope of the diffractive pattern.[7-12] Such calculations have been given in Refs. 8, 9, 11, and 12 and the predictions of Eqs. (42), (43), (44), and (50) have been compared to these published results and good agreement is obtained for the heavy nuclei considered here. Of course, the predictions of Eq. (50) and the corresponding calculations of Harrington and Varma[8] disagree because the latter show corrections due to the spurious center-of-mass motion.

Some general comments about the effects of correlations on proton-nucleus cross sections are appropriate. First, allowing k_F to vary with positions as in Eq. (29) results in about 50–100% larger increases at the diffractive maxima than if k_F were fixed to 1.36 fm^{-1}. Second, *no* angle shift in the positions of the maxima result from these $\sim\rho^2$ corrections, even at large momentum transfers (~3–4 fm^{-1}). Third, the realistic center-of-mass transformation correction included here [Eq. (50)] is much smaller than the spurious c.m. correction calculated by Harrington and Varma[8] and by Alkhazov.[12] Finally, the effects of these correlation terms on the proton-nucleus analyzing power, $A_y(\theta)$, are rather small. These second-order terms lower the $A_y(\theta)$ at forward angles and raise it at back angles, typically by only about 0.02 to 0.05, the spin-independent correlation terms, Eqs. (42), (43), (44), and (50) tending to have about the same effect as the spin-dependent correction, Eq. (56) itself. Since these effects are small and move the predicted result for $A_y(\theta)$ *away* from the data one must conclude, as was previously noted in Sec. IIA, that more flexible forms for $t^s_{pj}(q^2)$ are needed.

The effects of all these correlation terms on the predicted proton-nucleus elastic cross sections have been calculated. The total percentage increase at each diffractive maximum due to all five correlation correction terms are as follows; for ^{40}Ca, increases of 13%, 18%, and 20% at the first, second, and third maxima are observed; for ^{116}Sn, the results are 8%, 13%, 17%, and 21% at the first four maxima; and for ^{208}Pb, 6%, 10%, 14%, 18%, and 23% increases are seen at the first five maxima, respectively. These are generally in good agreement with Chaumeaux *et al.*,[11] are smaller than Harrington and Varma's result[8] (due to their inclusion of the spurious center-of-mass correction) and are larger than the effects calculated by Boridy and Feshbach[9] since they fix $k_F = 1.36$ fm^{-1}. These calculations and those in Ref. 9 would agree however if $k_F = 1.36$ fm^{-1} were assumed here, rather than Eq. (29).

The relative importance of each of these five corrections is given in Table III. The values here indicate the percentage of the total correlation effect (increase of the diffractive maxima) due to each correction term in Eq. (57) acting separately. Positive (negative) signs indicate that the values of the diffractive maxima in the proton-nucleus cross sections have increased (decreased). These percentages are based on the changes in the strengths of the maxima in the proton-nucleus diffractive patterns. As expected, the Pauli correction dominates. The effect of including correlations on the deduced values of the neutron rms radii can be estimated by fitting the angular distribution data, with and without these terms. For ^{40}Ca, ^{116}Sn, and ^{208}Pb the neutron radii increase about 0.05, 0.02, and 0.01 fm, respectively.[11] The principal variation in the neutron geometry is an increase in the diffuseness.

D. Details of the error analysis

The specific details and results of the uncertainty in the deduced neutron distributions and rms radii due to statistical error, model dependence, and various theoretical and experimental errors have been discussed previously,[6] so only a brief summary will be given here.

Initially, all data are fit as discussed throughout this section by assuming a specific model for the neutron density, namely

$$\rho_n^{(0)}(r) = \rho_{on}(1+w_n r^2/R_n^2)/\{1+\exp[(r^k-R_n^k)/Z_n^k]\}, \quad (58)$$

where k can equal either 1 or 2. Having obtained the best possible fit to the proton-nucleus elastic

TABLE III. Relative importance of the various correlation correction terms discussed in the text. Values are percentages of the total increase in the magnitude of the maxima in the differential cross sections due to each correlation term acting separately. Positive signs indicate an increase in the cross section, while negative signs denote decreases. Averages of values at the first several maxima are used to obtain these percentages.

Nucleus	Pauli %	SRD %	PSR–I %	c.m. %	Pauli–S.O. %
^{40}Ca	85.0	10.0	−2.1	11.0	−3.9
^{116}Sn	91.3	11.6	−2.4	5.2	−5.7
^{208}Pb	92.2	11.7	−2.8	3.4	−4.5

scattering data the neutron density is then generalized to

$$\rho_n(r) = b[\rho_n^{(0)}(r) + S\delta\rho_n(r)], \tag{59}$$

where[22]

$$\delta\rho_n(r) = (2\pi^{3/2}\gamma^3)^{-1}\sum_{i=1}^{W} Q_i(1+2c_i^2/\gamma^2)^{-1} \times\{\exp[-(r-c_i)^2/\gamma^2] + \exp[-(r+c_i)^2/\gamma^2]\}. \tag{60}$$

The strengths, Q_i, and the positions , c_i, of the Gaussians in $\delta\rho_n(r)$ are selected at random and the overall strength S is increased until the fit to the angular distribution deteriorates. Approximately fifty densities, $\rho_n(r)$, are generated in this way for each case. The number of Gaussians, W, is 12 or less[6,22,53,62] and $0 \leq Q_i \leq 1$ and $0 \leq c_i \leq 2R_n$.[6] The constant b is adjusted for each density to ensure proper normalization. The width parameter, γ, is limited by the finite nucleon size or by the smallest oscillatory structure observed in Hartree-Fock wave functions[38,63] and is here assumed to be 1.39 fm.[53] Finally, $\rho_n(r) \geq 0$ is required.

The criterion for determining S is[6]

$$\left|\frac{d\sigma}{d\Omega_k}(\text{theory},\ S\neq 0) - \frac{d\sigma}{d\Omega_k}(\text{exp})\right| - \left|\frac{d\sigma}{d\Omega_k}(\text{theory},\ S=0) - \frac{d\sigma}{d\Omega_k}(\text{exp})\right| = \Delta\sigma_{\text{exp},k}, \tag{61}$$

where $d\sigma/d\Omega_k(\text{theory})$, $d\sigma/d\Omega_k(\text{exp})$, and $\Delta\sigma_{\text{exp},k}$ are the theoretical and experimental cross sections and the experimental statistical error, respectively, at the kth data point in the angular distribution. The strength S is increased until this equation is satisfied at some data point. This technique evaluates the uncertainty in $\rho_n(r)$ due to statistical error in the data and due to that error caused by the fact that the experimental data extend only to finite momentum transfer.

Uncertainties in the neutron density caused by systematic errors such as those in the (1) absolute normalization and scattering angle of the data; (2) proton density; (3) incident beam energy and polarization; (4) nucleon-nucleon parameters for a given discrete solution (see Sec. IIA); and, (5) estimates for the second-order correlation terms are evaluated by individually varying each of these inputs, recovering the fit to the elastic data by varying the neutron surface geometry, and noting the change in the rms radius.[6] The results based on first-order calculations for several nuclei are given in Refs. 5 and 6. Since correlations are included in the present analysis, the uncertainty in the deduced neutron matter radius is reduced from the value of ±0.07 fm in Refs. 5 and 6 to about ±0.05 fm. Of course this estimate assumes a particular solution to the two-nucleon data. As was pointed out in Sec. IIA, radius differences of about 0.2 fm can occur if one adopts different discrete solutions for the N-N amplitudes, and it is emphasized that the quoted errors of ±0.05 fm here or ±0.07 fm in the earlier first-order analysis[5,6] do not make allowance for these discrete ambiguities.

A list of several higher-order corrections not included here will close this section. Virtual charge exchange induced by the isovector part of the N-N amplitude has not been computed here, but has been shown to be very small at these energies by Harrington and Varma.[8] Long range correlations involving virtual excitation to low lying nuclear collective states is largely taken into account already in these second-order calculations.[11] The remaining correction has been shown to be very small for ^{40}Ca by Abgrall[64] for $q < 2.5$ fm^{-1}. Contributions of the double-spin-flip amplitudes which enter only in the second-order potential are totally negligible.[65] Intermediate *nucleon* excited states[65,66] are supposed to have the effect of filling in the minima of the diffractive angular distribution and would be absorbed into the large uncertainty in the α_{pj} parameters of the N-N amplitudes and would not have significant effects on the deduced neutron density. Projectile-target antisymmetrization[67] as well as Fermi-motion averaging[68,69] have been shown to be quite insignificant. Third-order terms are also quite small.[8,19] Nonlocality effects should also be considered, but are generally believed to be negligible for proton scattering at intermediate energies.[17,70,71] Finally, corrections due to exchange currents[72] are not explicitly included. All of these corrections are small relative to the Pauli correlation correction, and at any rate would tend to cancel out when relative differences of neutron densities are computed as is done here. The numerical results of the calculations described in this section will now be given.

III. RESULTS OF THE ANALYSIS

The elastic angular distribution and analyzing power data, $A_y(\theta)$, have been studied using the optical potential of Eq. (57) with the proton densities having been derived from empirical charge densities[49-53] using Eq. (13). These data were then simultaneously fit by varying the parameters of the neutron model density in Eq. (58) and the isospin averaged, spin-dependent parameters $\bar{\theta}_p$ and $\bar{\alpha}_{sp}$ (see Sec. IIA). The fits to the elastic angular distributions are generally extremely similar to the previously published first-order results[1-6] and so will not be repeated again here. Some improvement in the fits to the back angle data is worth

TABLE IV. Best fit neutron density parameters, isospin averaged spin dependent parameters, and rms radii of the neutron, proton, and charge densities as derived from the second-order calculations discussed in Sec. II.

Nucleus	w_n	R_n fm	Z_n fm	k	$\langle r_n^2\rangle^{1/2}$ fm	$\langle r_p^2\rangle^{1/2}$ fm	$\langle r_{ch}^2\rangle^{1/2}$ fm	$\bar{\theta}_p$ fm^2	$\bar{\alpha}_{sp}$	$\bar{B}_{sp}$ fm^2
^{40}Ca	−0.082	3.48	0.64	1	3.491	3.392	3.482	10.8	0.60	0.2
^{48}Ca	0.078	3.85	0.53	1	3.625	3.396	3.470	8.6	0.70	0.2
^{58}Ni	0.13	3.90	0.54	1	3.700	3.686	3.772	9.9	0.60	0.2
^{64}Ni	0.28	3.88	0.60	1	3.912	3.745	3.845	9.6	0.70	0.2
^{116}Sn	0.31	4.72	2.86	2	4.692	4.546	4.619	8.8	0.73	0.2
^{124}Sn	0.45	4.96	2.86	2	4.851	4.599	4.670	8.4	0.71	0.2
^{208}Pb	0.33	5.93	3.28	2	5.611	5.453	5.503	8.2	0.69	0.2

mentioning, however. For ^{40,48}Ca and ^{58}Ni the first-order results[3,4] at back angles ($\theta_{c.m.} \gtrsim 18°$) are shifted inward in angle and are too low in magnitude. Best fits using the second-order optical potential can remove some of this discrepancy.

The best fits obtained to the proton-nucleus analyzing powers with the second-order calculations are slightly worse than those of the first-order calculations. As stated in Sec. IIC the predicted $A_y(\theta)$ is lowered at forward angles and the maxima are raised at back angles. A partial recovery of the fits in second-order can be obtained by reducing the imaginary part of the spin-orbit potential, i.e., increasing $\bar{\alpha}_{sp}$ but keeping $(\bar{\theta}_p\bar{\alpha}_{sp})$ constant. The typical changes in $\bar{\alpha}_{sp}$ and $\bar{\theta}_p$ from the values empirically deduced via first-order calculations are +0.1 and −2 fm^2, respectively. In the final fits the first maximum is lowered by 0.025 for ^{40}Ca and 0.012 for ^{124}Sn, while the last maximum is raised 0.10 for ^{40}Ca and 0.03 for ^{124}Sn. The correlation effects decrease with increasing target mass. For the study of neutron densities, which is the primary interest here, such differences in the quality of the fit to the $A_y(\theta)$ data are insignificant, since the entire spin-orbit potential itself has only a perturbative effect on $\rho_n(r)$.[5]

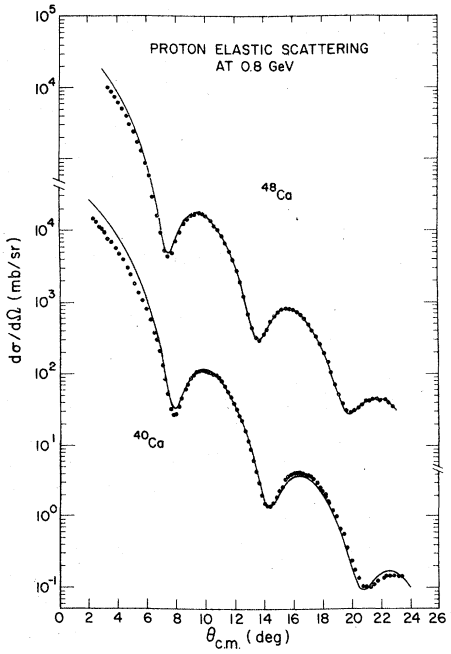

FIG. 6. Theoretical second-order optical potential fits and experimental elastic angular distribution data for polarized protons on ^{40,48}Ca at 0.8 GeV. Statistical errors are generally smaller than the plotted points.

The values of the neutron density parameters, $\bar{\theta}_p$ and $\bar{\alpha}_{sp}$ which provide the best fits to the $p+A$ data as well as the neutron and proton point density rms radii are given in Table IV. The second-order calculations for ^{40,48}Ca are shown in Fig. 6. The improved quality of the fit at back angles can be seen by comparing these fits to those in Ref. 4. The poor agreement between theory and experiment at the very forward angles ($\lesssim 7°$) for ^{40}Ca has recently been determined to be due to experimental difficulties[73] so that the very forward angle data

TABLE V. Neutron-proton and neutron isotopic differences as deduced by the second-order analysis presented here and as predicted by the density matrix expansion variant of Hartree-Fock theory. All values are in Fermis. The deduced Δr_{np} values are uncertain by ±0.05 fm and the errors in $\Delta r_{nn'}$ given here are explained in the text.

Nucleus	Deduced Δr_{np}	Deduced $\Delta r_{nn'}$	DME Δr_{np}	DME $\Delta r_{nn'}$
^{40}Ca	0.10		−0.05	
^{48}Ca	0.23	0.13 ± 0.04	0.19	0.26
^{58}Ni	0.01		0.00	
^{64}Ni	0.17	0.21 ± 0.02	0.13	0.18
^{116}Sn	0.15		0.12	
^{124}Sn	0.25	0.16 ± 0.02	0.21	0.13
^{208}Pb	0.16		0.20	

shown here were not included in the $|\chi|^2$ minimization procedure. Only ^{40,48}Ca are analyzed here since the principal interest is to make detailed comparisons of neutron density shapes and rms radii with Hartree-Fock predictions, which should be quite good for ^{40,48}Ca,[38,63] but less reliable for ^{42,44}Ca.

In Table V the final values for $\Delta r_{np} \equiv \langle r_n^2 \rangle^{1/2} - \langle r_p^2 \rangle^{1/2}$ and for $\Delta r_{nn'} \equiv \langle r_n^2(N', Z) \rangle^{1/2} - \langle r_n^2(N, Z) \rangle^{1/2}$ are given. As stated in Sec. IID the error in Δr_{np} is about ±0.05 fm. The uncertainties which contribute to the error in $\Delta r_{nn'}$ are the statistical error and model dependence of the deduced neutron densities and the error in the charge densities. Adding each of these uncertainties in quadrature, one obtains an uncertainty in $\Delta r_{nn'}$ of ±0.04, ±0.02, and ±0.02 fm for the ^{40,48}Ca, ^{58,64}Ni, and ^{116,124}Sn differences, respectively. Also given in Table V are the corresponding quantities as predicted by the density matrix expansion (DME) code of Negele.[38] The agreement is very good in all cases, except for ^{40}Ca. The $r_n(^{48}\text{Ca}) - r_n(^{40}\text{Ca})$ difference is usually found to be about 0.17 ± 0.04 fm[4,11,13,45] from analyses of proton scattering data, in disagreement with the 0.25 fm typically predicted by Hartree-Fock calculations.[4,38,63] The values of Δr_{np} obtained here for the ^{40,48}Ca LAMPF data[4] are generally about 0.08 fm larger than that determined by analyses of the 1.04 GeV Saclay data.[11] Plans are underway at LAMPF to retake these calcium data,[73] and it is possible that the overall normalization could change and this 0.08 fm discrepancy be largely removed. Even if such a renormalization of the calcium data should result, the $r_n(^{48}\text{Ca}) - r_n(^{40}\text{Ca})$ difference would remain essentially unchanged.

The deduced neutron density error envelopes have been computed for each of these nuclei as discussed in Sec. IID and in Ref. 6. The results are shown in Figs. 7–9. The shaded regions in the upper halves of these figures encompass all the neutron densities randomly generated according to Eqs. (59)–(61). The dashed curves are the point neutron densities predicted by the DME code.[38] The best agreement here is obtained for ^{48}Ca and ^{116,124}Sn. In all cases the DME densities are slightly too diffuse compared with the deduced

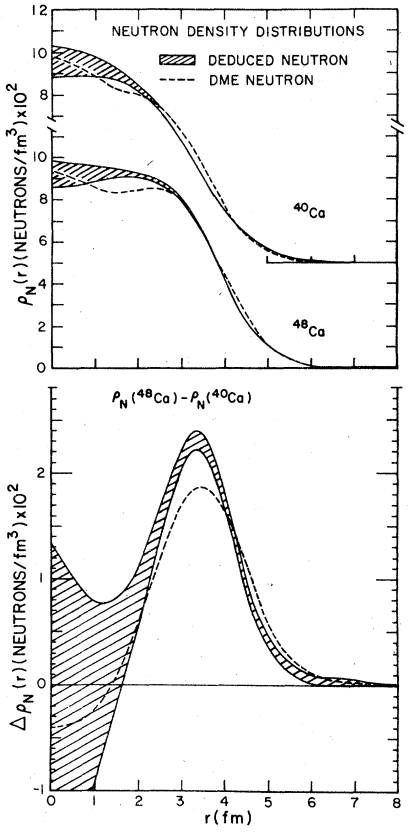

FIG. 7. Point neutron density distributions for ^{40,48}Ca deduced from the second-order KMT analysis (shaded bands) and predicted by the density matrix expansion approach to Hartree-Fock theory (dashed curves) as discussed in the text. The difference between the ^{48}Ca and ^{40}Ca deduced neutron densities is compared with the difference predicted by the DME code of Negele in the lower half.

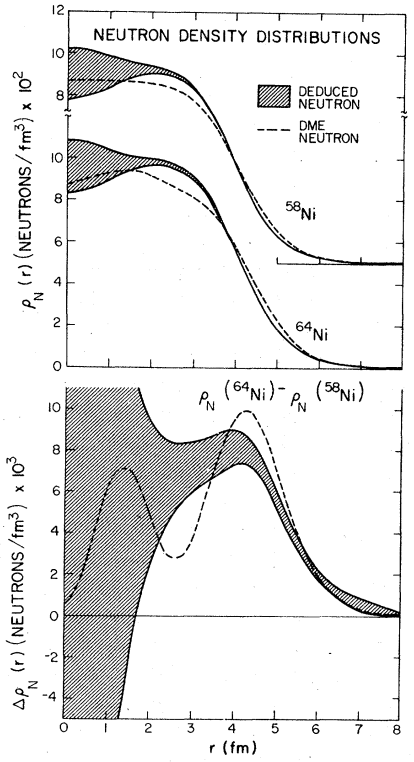

FIG. 8. The same as in Fig. 7, but for ^{58,64}Ni.

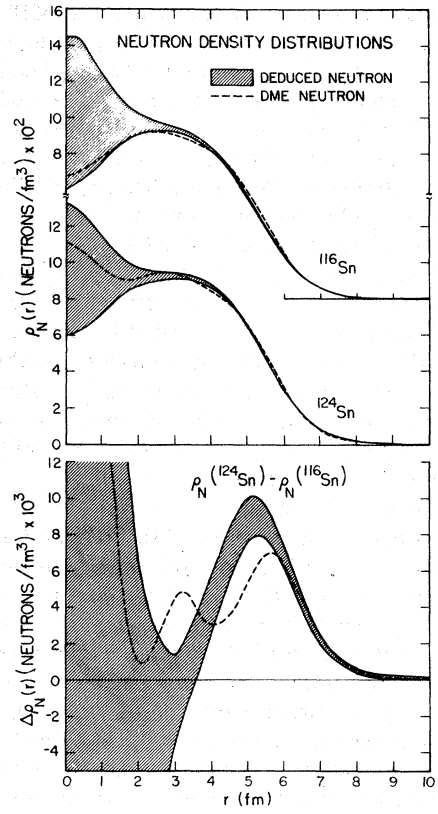

FIG. 9. The same as in Fig. 7, but for ^{116,124}Sn.

densities. The shaded envelopes in the upper halves of these figures account for statistical and model dependence errors only.

In the lower halves of Figs. 7–9 the neutron difference envelopes and DME predictions are compared for ^{40,48}Ca, ^{58,64}Ni, and ^{116,124}Sn, respectively. For the ^{40,48}Ca and ^{58,64}Ni differences the statistical and model-dependence errors are added in quadrature with the proton density error envelope as obtained from analyses of electron scattering and muonic atom data,[54] this proton error being weighted by Z/N before being added to the neutron statistical error envelope. For the ^{116,124}Sn comparison, no proton density error envelopes were available, but based on the effects this error has upon the ^{40,48}Ca and ^{58,64}Ni difference envelopes, the difference band in Fig. 9 should be about 50% wider for $r \gtrsim 3$ fm. No error band is given for the DME predictions since the dashed curves are only intended to qualitatively indicate the nature of Hartree-Fock predictions. The general agreement is good for all three cases. Because of the reduced errors for $\Delta r_{nn'}$ due to the cancellation of systematic errors as discussed in Sec. II, the relative difference comparisons in Table V and in Figs. 7–9 offer a sensitive test of Hartree-Fock theory.

IV. SUMMARY AND CONCLUSIONS

In this work a careful effort has been made to calculate accurately the relative differences between deduced neutron rms radii and between density distributions of various isotopes using the Kerman, McManus, and Thaler theory of the optical potential. Comparisons with typical Hartree-Fock predictions, namely those of the density matrix expansion approach,[38] have also been presented. Ambiguities in fitting the two-nucleon cross section and polarization data and uncertainties as to the importance of double-spin-flip amplitudes have been pointed out as being the prime motivation for concentrating for the present on these relative difference comparisons. Electromagnetic corrections to the proton density have been explicitly included as have the major second-order terms in the proton-nucleus optical potential, both for the central and the spin-orbit parts. Approximately model-independent densities have been used for the neutron densities in order to estimate the uncertainty in the deduced neutron distribution and radius due to statistical and model-dependence errors. Other systematic sources of error have been included from which a total error for the absolute and relative neutron radii are obtained. It is seen that the electromagnetic and correlation corrections are both small and each tends to cancel the other's effect on the deduced neutron radii. Therefore, the earlier first-order calculations do provide good estimates of Δr_{np}, $\Delta r_{nn'}$, and $\rho_n(r)$ within the stated errors of these analyses.[2-6]

From the generally good agreement with Hartree-Fock predictions found here and elsewhere[2-6,11,45] for the deduced values of Δr_{np}, one should not expect the uncertainties and ambiguities with the two-nucleon amplitudes discussed in Sec. II A to be too serious. However, until the two-nucleon amplitudes are completely determined at energies near 1 GeV, final KMT values for Δr_{np} cannot be given and the errors quoted for Δr_{np} can only be computed as given here and in Ref. 6. The point to be emphasized here is that reliable measures of the isotopic differences between neutron densities and radii can be made as long as reasonable estimates for the spin-independent N-N amplitudes are used. Thus for now at least, these isotopic density and radii differences pose the most severe tests for the Hartree-Fock predictions of neutron matter densities.

ACKNOWLEDGMENTS

The author would like to thank Dr. W. R. Coker for carefully reading the manuscript and for numerous helpful discussions and comments regarding this work. Thanks is also expressed to Dr. J. Friar for helpful discussions regarding the electromagnetic corrections. This research was supported in part by the U. S. Department of Energy.

[1]G. W. Hoffmann *et al.*, Phys. Rev. Lett. 40, 1256 (1978).
[2]G. W. Hoffmann *et al.*, Phys. Lett. 76B, 383 (1978).
[3]G. W. Hoffmann *et al.*, Phys. Lett. 79B, 376 (1978).
[4]G. Igo *et al.*, Phys. Lett. B (to be published).
[5]L. Ray, G. W. Hoffmann, G. Blanpied, W. R. Coker, and R. P. Liljestrand, Phys. Rev. C 18, 1756 (1978).
[6]L. Ray, W. R. Coker, and G. W. Hoffmann, Phys. Rev. C 18, 2641 (1978).
[7]G. K. Varma and L. Zamick, Nucl. Phys. A306, 343 (1978).
[8]D. R. Harrington and G. K. Varma, Nucl. Phys. A306, 477 (1978).
[9]E. Boridy and H. Feshbach, Ann. Phys. (N.Y.) 109, 468 (1977).
[10]V. Layly and R. Schaeffer, Phys. Rev. C 17, 1145 (1978).
[11]A. Chaumeaux, V. Layly, and R. Schaeffer, Ann. Phys. (N.Y.) 116, 247 (1978).
[12]G. D. Alkhazov, Nucl. Phys. A280, 330 (1977).
[13]G. D. Alkhazov *et al.*, Nucl. Phys. A274, 443 (1976).
[14]G. D. Alkhazov *et al.*, Phys. Lett. 67B, 402 (1977).
[15]R. Bertini *et al.*, Phys. Lett. 45B, 119 (1973).
[16]G. D. Alkhazov *et al.*, Phys. Lett. 57B, 47 (1975); Report No. LINP-244, Leningrad, 1976 (unpublished).
[17]A. K. Kerman, H. McManus, and R. M. Thaler, Ann. Phys. (N.Y.) 8, 551 (1959).
[18]H. Feshbach, A. Gal, and J. Hüfner, Ann. Phys. (N.Y.) 66, 20 (1971).
[19]J. J. Ullo and H. Feshbach, Ann. Phys. (N.Y.) 82, 156 (1974).
[20]W. Bertozzi, J. Friar, J. Heisenberg, and J. W. Negele, Phys. Lett. 41B, 408 (1972).
[21]J. L. Friar and J. W. Negele, in *Advances in Nuclear Physics*, edited by M. Barranger and E. Vogt (Plenum, New York, 1975), Vol. 8, p. 219.
[22]I. Sick, Nucl. Phys. A218, 509 (1974).
[23]R. J. Glauber, in *Lectures in Theoretical Physics*, edited by W. E. Brittin and L. G.Dunham (Interscience, New York, 1959), p. 315; see also *High Energy Physics and Nuclear Structure*, edited by G. Alexander (North-Holland, Amsterdam, 1967), p. 311; and *High Energy Physics and Nuclear Structure*, edited by S. Devons (Plenum, New York, 1970), p. 207.
[24]M. J. Moravcsik, *The Two-Nucleon Interaction* (Clarendon, Oxford, 1963), pp. 11–18.
[25]J. Bystricky, F. Lehar, and Z. Janout, Saclay Report No. CEA-N-1547(E), 1972 (unpublished).
[26]O. Benary, L. R. Price, and G. Alexander, Lawrence Berkeley Laboratory Report No. UCRL-20000NN, 1970 (unpublished).
[27]H. B. Willard, *et al.*, Phys. Rev. C 14, 1545 (1976).
[28]P. R. Bevington *et al.*, Phys. Rev. Lett. 41, 384 (1978).
[29]R. Carlini *et al.*, Phys. Rev. Lett. 41, 1341 (1978).
[30]V. P. Dzhelepov, B. M. Golovin, V. S. Nadezhdin, and V.I. Satarov, Proceedings of the Twelfth International Conference on High Energy Physics, Dubna, 1964 (Atomizdat, Moscow, 1966), Vol. 1, p. 11.
[31]M. L. Marshak *et al.*, Phys. Rev. C 18, 331 (1978).
[32]T. J. Devlin *et al.*, Phys. Rev. D 8, 136 (1973).
[33]A. A. Vorobyov *et al.*, Phys. Lett. 41B, 639 (1972).
[34]O. V. Dumbrais, Sov. J. Nucl. Phys. 13, 626 (1971).
[35]G. J. Igo, Rev. Mod. Phys. 50, 523 (1978).
[36]W. Grein and P. Kroll (unpublished).
[37]A. A. Carter and D. V. Bugg, Phys. Lett. 20, 203 (1966).
[38]J. W. Negele and D. Vautherin, Phys. Rev. C 5, 1472 (1972); The DME code of Negele provided the numerical results given here.
[39]W. R. Coker, L. Ray, and G. W. Hoffmann, Phys. Lett. 64B, 403 (1976).
[40]E. Lambert and H. Feshbach, Ann. Phys. (N.Y.) 76, 80 (1973).
[41]C. R. Schumacher and H. A. Bethe, Phys. Rev. 121, 1534 (1961).
[42]W. de Boer *et al.*, Phys. Rev. Lett. 34, 558 (1975).
[43]I. P. Auer *et al.*, Phys. Lett. 67B, 113 (1977).
[44]A. Chaumeaux, V. Layly, and R. Schaeffer, Phys. Lett. 72B, 33 (1977).
[45]G. K. Varma and L. Zamick, Phys. Rev. C 16, 308 (1977).
[46]G. Adams *et al.* (to be published).
[47]G. Höhler *et al.*, Nucl. Phys. B114, 505 (1976).
[48]T. Tamura, W. R. Coker, and F. Rybicki, Comp. Phys. Commun. 2, 94 (1971).
[49]B. B. P. Sinha, G. A. Peterson, R. R. Whitney, I. Sick, and J. S. McCarthy, Phys. Rev. C 7, 1930 (1973).
[50]J. B. Bellicard *et al.*, Phys. Rev. Lett. 19, 527 (1967).
[51]I. Sick *et al.*, Phys. Rev. Lett. 35, 910 (1975); and private communication.
[52]J. R. Ficenec, L. A. Fajardo, W. P. Trower, and I. Sick, Phys. Lett. 42B, 213 (1972).
[53]B. Frois *et al.*, Phys. Rev. Lett. 38, 152 (1977).
[54]H. D. Wohlfahrt, private communication.
[55]I. Ahmad, Nucl. Phys. A247, 418 (1975).
[56]J. P. Auger, J. Gillespie, and R. J. Lombard, Nucl. Phys. A262, 372 (1976).
[57]S. J. Wallace (unpublished).
[58]J. Yvon, *Correlations and Entropy in Classical Statistical Mechanics* (Pergamon, Oxford, 1969).
[59]A. de Shalit and H. Feshbach, *Theoretical Nuclear Physics* (Wiley, New York, 1974), pp. 135–140.
[60]P. Signell, in *Advances in Nuclear Physics*, edited by M. Barranger and E. Vogt (Plenum, New York, 1969), Vol. 2, p. 223.
[61]E. Kujawski and J. P. Vary, Phys. Rev. C 12, 1271 (1975).
[62]I. Brissaud and M. K. Brussel, Phys. Rev. C 15, 452 (1977).
[63]J. W. Negele, Phys. Rev. C 1, 1260 (1970).
[64]Y. Abgrall, J. Labarsouque, B. Morand, and E. Caurier, private communication; Aussois Meeting, 1977; and discussion in Ref. 11.
[65]S. J. Wallace and D. A. Sparrow, private communication.
[66]S. J. Wallace and Y. Alexander, Phys. Rev. Lett. 38, 1269 (1977).
[67]R. R. Scheerbaum, Phys. Rev. C 7, 2166 (1973).
[68]S. J. Wallace, Phys. Rev. C 12, 179 (1975).
[69]L. Ray and W. R. Coker, Phys. Rev. C 16, 340 (1977).
[70]F. Perey and B. Buck, Nucl. Phys. 32, 353 (1962).
[71]N. Azziz, Nucl. Phys. A147, 401 (1970).
[72]J. W. Negele and D. O. Riska, Phys. Rev. Lett. 40, 1005 (1978).
[73]G. W. Hoffmann, private communication.